Geometrical Heterogeneity Dominates Thermal Fluctuations in Facilitating Chromatin Contacts

Bruno Beltran[1,*] Deepti Kannan[2,*] Quinn MacPherson[2] and Andrew J. Spakowitz[3,4,5,†]

[1]*Biophysics Program, Stanford University, Stanford, California 94305, USA*
[2]*Department of Physics, Stanford University, Stanford, California 94305, USA*
[3]*Chemical Engineering Department, Stanford University, Stanford, California 94305, USA*
[4]*Department of Materials Science and Engineering, Stanford University Stanford, California 94305, USA*
[5]*Department of Applied Physics, Stanford University, Stanford, California 94305, USA*

Within a living cell, the myriad of proteins that bind DNA introduce heterogeneously spaced kinks into an otherwise semiflexible DNA double helix. To investigate the effects of heterogeneous nucleosome binding on chromatin organization, we extend the wormlike chain model to include statistically spaced, rigid kinks. On timescales where nucleosome positions are fixed, we find that the probability of chromatin loop formation can vary by up to six orders of magnitude between two sets of nucleosome positions drawn from the same distribution. On longer timescales, we show that continuous rerandomization due to nucleosome turnover results in chromatin tracing out an effective WLC with a dramatically smaller Kuhn length than bare DNA. Together, these observations demonstrate that nucleosome spacing acts as the primary source of the structural heterogeneity that dominates local and global chromatin organization.

The spatial organization of chromatin—genomic DNA and its associated proteins—is critical to many biological processes, from controlling gene expression [1] to facilitating DNA damage repair [2,3]. The fundamental unit of eukaryotic chromatin organization is the nucleosome, which consists of 147 basepairs of DNA wrapped around a histone-protein octamer [4]. Linker DNA connecting adjacent nucleosomes ranges from less than 10 bp on average in fission yeast [5] to more than 80 bp in sea urchin sperm cells [6].

In vitro images of chromatin have historically contained regular, "30-nm fiber" helical structures, motivating models of chromatin with constant nucleosome spacing [7–17]. However, recent measurements indicate that *in vivo*, interphase mammalian chromatin instead forms a disordered, "beads-on-a-string" structure [18–20]. Additionally, modern *in vivo* nucleosome positioning data suggest that linkers are extremely heterogeneous. The occupancy profiles of even the most well-positioned nucleosomes—such as those near transcription start sites—are well described by a model where nucleosomes bind uniformly along the DNA [12,21–31] and are merely excluded from certain areas [32].

Previous works addressing linker length heterogeneity are either simulation studies [33,34] or purely geometrical models [35,36]. These models can produce individual "beads-on-a-string" configurations qualitatively similar to those observed in bulk chromatin. However, there remains a need for an analytical approach that can systematically characterize how and when linker length heterogeneity leads to structural disorder.

In this Letter, we present a model combining thermal fluctuations in the DNA linkers with the geometric effects of experimentally relevant linker length heterogeneity. We show that almost any linker length heterogeneity is sufficient to produce the disordered chromatin structures that are now believed to dominate nuclear architecture. The intuition behind our structural claims extends to any polymer composed of aperiodic kinks, such as the dihedral "kinks" found at junctions of block copolymers. More broadly, our results contribute to a large class of problems in which quenched disorder competes with thermal fluctuations to determine the structural properties of a system.

We model each DNA linker as a twistable wormlike chain (TWLC), and the nucleosomes as the points where these linker strands connect. We label the orientation of the DNA entering the ith nucleosome by the matrix $\Omega_{\text{entry}}^{(i)} \in SO(3)$. The exit orientation $\Omega_{\text{exit}}^{(i)}$ must then satisfy $\Omega_{\text{exit}}^{(i)} = \Omega_{\text{entry}}^{(i)}\Omega_{\text{kink}}$, where Ω_{kink} is the fixed kink rotation shown in Fig. 1.

We represent a TWLC of length L as a space curve $\vec{R}(s)$, $s \in [0, L]$. The chain's orientation at each point along this curve, $\Omega(s)$, is represented by an orthonormal triad $\vec{t}_i$, where $\vec{t}_3 = \partial_s \vec{R}(s)$. We track the bend and twist of our polymer via the angular "velocity" vector $\vec{\omega}(s)$, which operates as $\partial_s \vec{t}_i(s) = \vec{\omega}(s) \times \vec{t}_i(s)$. The Green's function

$$G_{\text{TWLC}}(\vec{R}, \Omega | \Omega_0; L_1) = \int_{\Omega(0)=\Omega_0}^{\Omega(s)=\Omega} \mathcal{D}[\Omega(s)] e^{-\beta\mathcal{E}} \delta\left(\vec{R} - \int_0^{L_1} \vec{t}_3 ds\right),$$
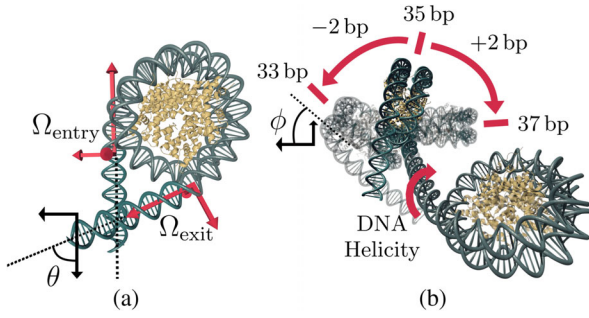
(1)

FIG. 1.   (a) The structure of a human nucleosome [37] with straight linkers extrapolated from the entry (Ω_{entry}) and exit (Ω_{exit}) orientations of the bound DNA. The amount of DNA wrapping the nucleosome dictates the spherical angle θ. (b) Two adjacent nucleosomes at zero temperature. The DNA double helix has an intrinsic twist density [$\tau = 2\pi/(10.5 \text{ bp})$], and the binding orientation of the histone octamer must align with the major groove of the double helix. Therefore, as the linker length L connecting two nucleosomes gets longer or shorter, the relative orientations of adjacent octamers change to create an angle $\phi = \tau L$.

of the first linker represents the probability that a polymer of length L_1 that begins at the origin with initial orientation Ω_0 ends at position $\vec{R}$ with end orientation Ω. For a TWLC with no kinks, the energy is quadratic in bending and twist deformations

$$\beta\mathcal{E} = \frac{l_p}{2}\int_0^{L_1} ds(\omega_1^2 + \omega_2^2) + \frac{l_t}{2}\int_0^{L_1} ds(\omega_3 - \tau)^2. \quad (2)$$

The natural twist of DNA gives $\tau = 2\pi(10.5 \text{ bp})^{-1}$, and we set the persistence length $l_p = 50$ nm and twist persistence length $l_t = 100$ nm to match measurements of DNA elasticity [38–41].

References [42] and [43] solve Eq. (1) analytically in Fourier space ($\vec{R} \rightarrow \vec{k}$) by computing the coefficients of the Wigner D-function expansion

$$\hat{G}_{\text{TWLC}}(\vec{k}, \Omega|\Omega_0; L_1) = \sum_{l;l_0 m_0 j_0} g_{l_0 m_0 j_0}^{l m_0 j_0} \mathcal{D}_l^{m_0 j_0}(\Omega)\mathcal{D}_{l_0}^{m_0 j_0 *}(\Omega_0).$$

$$(3)$$

To account for Ω_{kink}, we rotate the final orientation of the linker DNA, $\Omega = \Omega_{\text{entry}}$, to Ω_{exit} using the formula

$$\mathcal{D}_l^{m_0 j_0}(\Omega\Omega_{\text{kink}}) = \sum_j \sqrt{\frac{8\pi}{2l+1}} \mathcal{D}_l^{m_0 j}(\Omega_{\text{kink}})\mathcal{D}_l^{j j_0}(\Omega). \quad (4)$$

The resulting Green's function combines the effects of a DNA linker and a nucleosome but is still a Wigner D-function expansion with modified coefficients $B_{l_0 m_0 j_0}^{l m_0 j}$ (first computed in Ref. [44] and similarly introduced in Ref. [45]). We present an alternative derivation in the Supplemental Material [46].

We extract Ω_{kink} as a function of the number of nucleotides bound to the histone core from x-ray crystallography [4,47,48] and cryo-electron microscopy [37,49–52] measurements. In what follows, we fix the wrapping level to that found in the crystal structure (147 bp). Using different values for the wrapping level rescales our results (see Supplemental Material [46], Figs. S3 and S10).

To compose monomers of the nucleosome chain with prescribed linker lengths, we perform an iterated convolution of the Green's functions for each nucleosome-linker pair. In Fourier space, this corresponds to multiplying the matrices $B_{l_0 m_0 j_0}^{l m_0 j}(L_i)$. A key property of our model is that the relative orientation of adjacent nucleosomes is not only determined by Ω_{kink} and the thermal fluctuations of the linker strand, but also by changing the length of the linker strand [as demonstrated in Fig. 1(b)]. Our propagator G takes this into account implicitly due to the inclusion of τ in Eq. (2).

We begin by computing the end-to-end distance $\sqrt{\langle R^2 \rangle}$ of the chain using the formula $\lim_{k\to 0}(\partial^n B_{000}^{000}/\partial k^n) = i^n\langle R^n \rangle$. From this, we extract the Kuhn length, $b = \lim_{N\to\infty}\langle R^2 \rangle / \sum_{i=0}^{N} L_i$, where a smaller Kuhn length corresponds to a more compact chain. For a WLC, $b = 2l_p$ and thus increases with the bending stiffness.

In Fig. 2(a), we plot $\sqrt{\langle R^2 \rangle}$ as a function of chain length for homogeneous chains of nucleosomes with 36 and 38 bp linkers. We compare these curves to the $\sqrt{\langle R^2 \rangle}$ of a TWLC with the same Kuhn length but without kinks. At short length scales, the slope of $\sqrt{\langle R^2 \rangle}$ for all chains is one, corresponding to rigid-rod behavior. At the persistence length, the bare WLC's slope smoothly transitions to $1/2$ (on a log-log scale), corresponding to random-walk behavior. In contrast, the homogeneous chain $\sqrt{\langle R^2 \rangle}$ jumps from that of bare DNA to that of the best-fit WLC, whose Kuhn length is dramatically smaller than twice the persistence length of bare DNA.

To build a geometric intuition for how the kinks create this modified Kuhn length, we compare the Kuhn lengths of homogeneous, fluctuating chains to their zero-temperature configurations, where the entire chain is composed of rigid-rod linkers. Every homogeneous chain at zero temperature forms a helix of nucleosomes. The rise per base pair of the helix is determined by the spherical angles θ and ϕ connecting adjacent linkers (see Fig. 1). The nucleosome structure fixes θ, but ϕ depends linearly on the linker length, and is 10.5 bp periodic due to the DNA's helicity. Select values of ϕ lead to more compact zero-temperature structures with a smaller rise per base pair. As seen in Fig. 2(b), the fluctuating structures with a smaller rise per base pair have smaller Kuhn lengths.

The 10.5 bp periodicity of ϕ as linker length changes leads to the periodicity in Fig. 2(b). As $L_i \rightarrow \infty$, the Kuhn length approaches that of bare DNA only slowly (see Supplemental Material [46], Fig. S4).

We next consider heterogeneous chains where the linker lengths are drawn uniformly from a range $\mu \pm \sigma$. In Fig. 3,
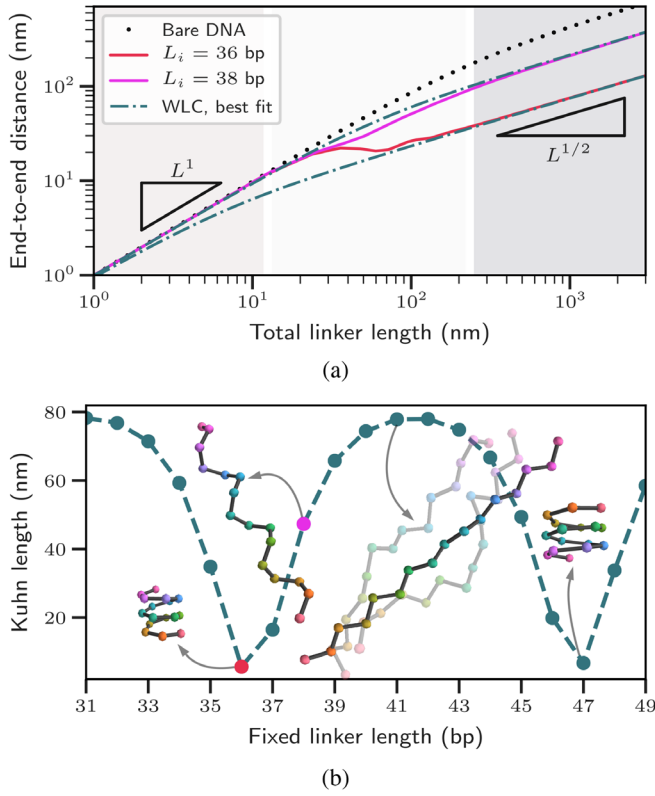
(a)

(b)

FIG. 2. (a) Average end-to-end distances for homogeneous chromatin chains with 36 and 38 bp linkers, compared to bare DNA and the best-fit WLCs. Rigid rod (L^1), Gaussian chain ($L^{1/2}$), and cross-over regimes highlighted. (b) Kuhn lengths of homogeneous chromatin chains are 10.5 bp periodic in linker length. Example zero-temperature chain configurations are shown, as well as two Monte Carlo (fluctuating) structures for the 41 bp case. Compact structures (36, 47 bp) have smaller Kuhn lengths than less compact structures (41 bp).

we see that as we increase σ, the zero-temperature configuration of the chain interpolates between a helix at $\sigma = 0$ and a random walk at larger σ. As a result, the zero-temperature structure itself has a Kuhn length, which describes the compactness of the random walk. As in the homogeneous case, the Kuhn length of the zero-temperature chain qualitatively predicts that of the fluctuating structure, as seen in Fig. 3. We find that even a single base pair of variance in nucleosome positions (see e.g., Supplemental Material [46], Fig. S5) can create enough geometric stochasticity at zero temperature to prevent the formation of regular fibers.

In the simplest model of nucleosome binding, nucleosomes bind uniformly randomly along the DNA [24], resulting in nucleosome spacings that are exponentially distributed (hereafter "the exponential chain"). While this picture ignores some details of *in vivo* nucleosome formation, Fig. 3 shows how any linker length distribution with sufficiently large variability (σ) exhibits behavior similar to the exponential chain. Thus, the results that
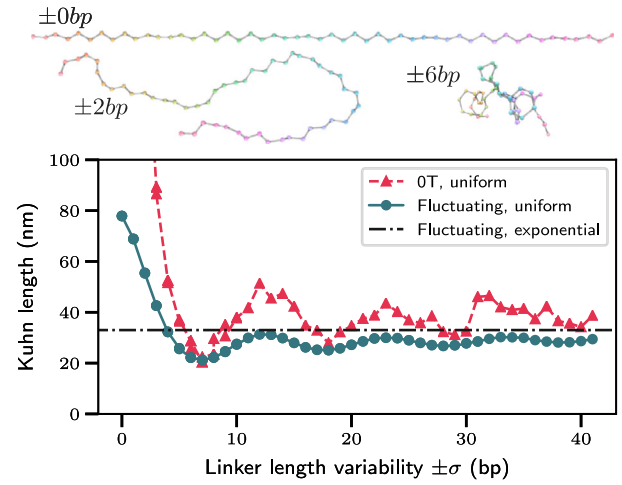

FIG. 3. Kuhn length of a heterogeneous chromatin chain with uniformly distributed linker lengths chosen from the range $\mu \pm \sigma$, where $\mu = 41$ bp. Example zero-temperature chains composed of rigid rod linkers are shown for $\sigma = 0$, 2, 6 bp. Kuhn length rapidly approaches that of the exponential chain (black line) in which linker lengths are exponentially distributed about the same μ.

follow are likely robust to adding more detail to the nucleosome binding model.

When averaged over the distribution of possible nucleosome positions, the end-to-end distance of our exponential chain takes the form of a WLC with a rescaled Kuhn length (see Supplemental Material [46], Fig. S6). This makes sense because at zero temperature, our model differs from a freely rotating chain only in the correlation between linker length and ϕ, and the freely rotating chain is known to converge to a wormlike chain under appropriate scaling [53]. We extract the rescaled Kuhn length as a function of $\langle L_i \rangle$ in Fig. 4.

Unlike the homogeneous case, where changing L_i selects between zero-temperature helices, increasing $\langle L_i \rangle$
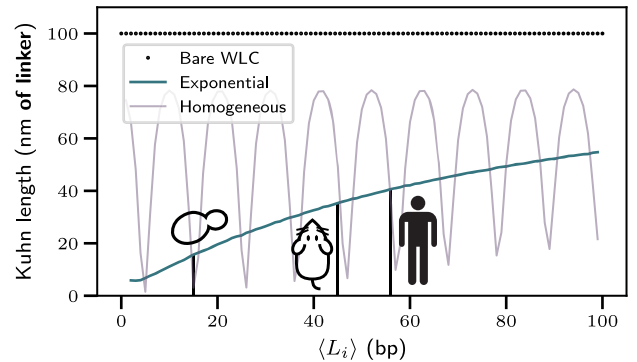

FIG. 4. Kuhn lengths of chromatin chains with exponentially distributed linkers as a function of the average linker length, which varies by cell type. Kuhn lengths for *S. cerevisiae* ($\langle L_i \rangle = 15$ bp), mice embryonic stem cells (45 bp), and human T cells (56 bp) are labeled.
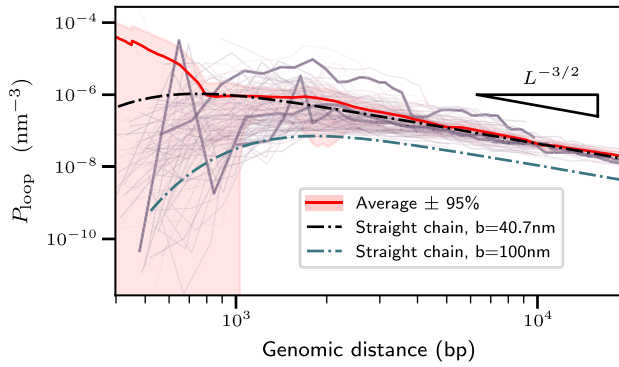
FIG. 5. Looping probabilities as a function of genomic separation for exponential chains. Each purple line designates an individual chain with linker lengths drawn from an exponential distribution with $\mu = 56$ bp. The red shaded area corresponds to 95% confidence intervals around the mean over the individual chains (red line). A wormlike chain (black dashed line) with the same Kuhn length as this average chain captures the looping probability for loops with at least three intervening nucleosomes. Three random individual chains are bolded.

in the heterogeneous case scales the zero-temperature random walk. As a result, Fig. 4 lacks the 10.5 bp periodicity of the homogeneous chain. Thus, for the purposes of coarse graining, an approximate knowledge of $\langle L_i \rangle$ should be sufficient to capture chromatin's average behavior as a WLC. A table of these Kuhn lengths is available in the Supplemental Material [46], Table S1.

To characterize the chain's structure on shorter length scales, we calculate the probability of genomic contacts (i.e., the looping probability). By numerically inverting the Fourier transform in Eq. (3), we can analytically evaluate $P_{\text{loop}} = G(\vec{R} = 0|L)$, a modified J factor with no orientational component. In Fig. 5, we plot this probability as a function of the loop size.

Strikingly, we observe that for a fixed genomic separation, different nucleosome spacings can change the contact probability by up to 6 orders of magnitude. The average looping probability, which is relevant at timescales where nucleosome positions can rerandomize, is captured well by a single WLC. Because of this effective WLC's reduced Kuhn length, we predict that chromatin's propensity for forming sub-kilobase-scale loops should be 1–4 orders of magnitude larger than that of bare DNA. The predicted looping propensity peaks at a length scale typical of promoter contacts *in vivo* and consistent with Hi-C looping data [54] (see Supplemental Material [46], Fig. S8). This result highlights how even without models of DNA more detailed than the WLC—for example those including DNA melting [55–57]—the propensity of small DNA loops can be enhanced by proteins that promote stochastically spaced kinks in the DNA.

Additionally, we find that the average looping probability is higher than that of most of the individual chains.

Thus, even an "informationless" chromatin remodeler that merely promotes random nucleosome repositioning can greatly facilitate subkilobase loop formation. At longer length scales, the looping probabilities approach the characteristic $L^{-3/2}$ Gaussian scaling. However, individual chains retain memory of their kinks, as indicated by how the highlighted chains persist above or below the average. Using a uniform linker length distribution leads to qualitatively similar results (see Supplemental Material [46], Fig. S9).

In conclusion, we provide rigorous justification for using an effective WLC to model *in vivo* chromatin. Because of the lack of experimental consensus on the persistence length l_p of chromatin [58], coarse-grained models of chromatin have historically used a range of values for l_p, sometimes even just using that of bare DNA [59–61]. We show that this choice leads to at least a twofold overestimation of the polymer's persistence length and a several orders-of-magnitude underestimation of looping at short length scales. Some past models have extracted a parameter that describes the linear compaction of chromatin (bp per nm of fiber) from Hi-C looping probabilities (see e.g., [62,63]). Our model's parameter-free estimate of chromatin's looping propensity provides a theoretical explanation for the effective Kuhn length predicted from these experimental measurements.

Our model excludes various important facets of chromatin's structure, such as interaction energies (sterics and stacking) and nucleosome "breathing." Since nucleosome breathing simply corresponds to choosing a different distribution for the angle $\theta \in [0, \pi]$ between adjacent nucleosomes, incorporating breathing leaves our results qualitatively unchanged (see Supplemental Material [46], Fig. S10). However, a more careful inclusion of breathing would likely require an explicit treatment of the effects of DNA sequence and linker histone on the nucleosome particle.

Our work highlights that the geometric effects of heterogeneous nucleosome binding dominate thermal fluctuations in driving chromatin contacts *in vivo*. Our insights into chromatin's bending stiffness will inform future studies on the effects of loop extrusion factors [61,64] and epigenetic states [60,64,65] on chromatin organization.

---

[*] These authors contributed equally to this work.
[†] ajspakow@stanford.edu

[1] M. R. Hübner, M. A. Eckersley-Maslin, and D. L. Spector, Curr. Opin. Genet. Dev. **23**, 89 (2013).

[2] M. H. Hauer and S. M. Gasser, Genes Dev. **31**, 2204 (2017).

[3] J. Stadler and H. Richly, Int. J. Mol. Sci. **18**, 1715 (2017).

[4] A. Cutter and J. J. Hayes, FEBS Lett. **589**, 2914 (2015).

[5] R. M. Givens, W. K. M. Lai, J. M. Rizzo, J. E. Bard, P. A. Mieczkowski, J. Leatherwood, J. A. Huberman, and M. J. Buck, Nucleic Acids Res. **40**, 7176 (2012).

[6] C. Spadafora, M. Bellard, J. Lee Compton, and P. Chambon, FEBS Lett. **69**, 281 (1976).

[7] S. A. Grigoryev, G. Bascom, J. M. Buckwalter, M. B. Schubert, C. L. Woodcock, and T. Schlick, Proc. Natl. Acad. Sci. U.S.A. **113**, 1238 (2016).

[8] N. Kepper, D. Foethke, R. Stehr, G. Wedemann, and K. Rippe, Biophys. J. **95**, 3692 (2008).

[9] E. Ben-Haïm, A. Lesne, and J.-M. Victor, Phys. Rev. E **64**, 051921 (2001).

[10] E. F. Koslover, C. J. Fuller, A. F. Straight, and A. J. Spakowitz, Biophys. J. **99**, 3941 (2010).

[11] J. Langowski and D. W. Heermann, Semin. Cell Dev. Biol. **18**, 659 (2007).

[12] O. Müller, N. Kepper, R. Schöpflin, R. Ettig, K. Rippe, and G. Wedemann, Biophys. J. **107**, 2141 (2014).

[13] H. Schiessel, W. M. Gelbart, and R. Bruinsma, Biophys. J. **80**, 1940 (2001).

[14] A. Scipioni, G. Turchetti, S. Morosetti, and P. De Santis, Biophys. Chem. **148**, 56 (2010).

[15] G. Wedemann and J. Langowski, Biophys. J. **82**, 2847 (2002).

[16] G. D. Bascom and T. Schlick, in *Nuclear Architecture and Dynamics*, Translational Epigenetics, Vol. 2, edited by C. Lavelle and J.-M. Victor (Academic Press, Boston, 2018), pp. 123–147.

[17] E. Koslover and A. J. Spakowitz, Soft Matter **9**, 7016 (2013).

[18] H. D. Ou, S. Phan, T. J. Deerinck, A. Thor, M. H. Ellisman, and C. C. O'Shea, Science **357**, eaag0025 (2017).

[19] M. A. Ricci, C. Manzo, M. F. García-Parajo, M. Lakadamyali, and M. P. Cosma, Cell **160**, 1145 (2015).

[20] T. Nozaki, R. Imai, M. Tanbo, R. Nagashima, S. Tamura, T. Tani, Y. Joti, M. Tomita, K. Hibino, M. T. Kanemaki, K. S. Wendt, Y. Okada, T. Nagai, and K. Maeshima, Mol. Cell **67**, 282 (2017).

[21] R. D. Kornberg and L. Stryer, Nucleic Acids Res. **16**, 6677 (1988).

[22] G. Chevereau, L. Palmeira, C. Thermes, A. Arneodo, and C. Vaillant, Phys. Rev. Lett. **103**, 188103 (2009).

[23] R. V. Chereji and A. V. Morozov, J. Stat. Phys. **144**, 379 (2011).

[24] D. A. Beshnova, A. G. Cherstvy, Y. Vainshtein, and V. B. Teif, PLoS Comput. Biol. **10**, e1003698 (2014).

[25] T. Chou, Phys. Rev. Lett. **99**, 058105 (2007).

[26] R. Kornberg, Nature (London) **292**, 579 (1981).

[27] T. N. Mavrich, I. P. Ioshikhes, B. J. Venters, C. Jiang, L. P. Tomsho, J. Qi, S. C. Schuster, I. Albert, and B. F. Pugh, Genome Res. **18**, 1073 (2008).

[28] W. Möbius and U. Gerland, PLoS Comput. Biol. **6**, e1000891 (2010).

[29] W. Möbius, B. Osberg, A. M. Tsankov, O. J. Rando, and U. Gerland, Proc. Natl. Acad. Sci. U.S.A. **110**, 5719 (2013).

[30] V. B. Teif and K. Rippe, J. Phys. Condens. Matter **22**, 414105 (2010).

[31] S. Tesoro, I. Ali, A. N. Morozov, N. Sulaiman, and D. Marenduzzo, Phys. Biol. **13**, 016004 (2016).

[32] E. A. Ozonov and E. van Nimwegen, PLoS Comput. Biol. **9**, e1003181 (2013).

[33] R. Collepardo-Guevara and T. Schlick, Proc. Natl. Acad. Sci. U.S.A. **111**, 8061 (2014).

[34] G. D. Bascom, T. Kim, and T. Schlick, J. Phys. Chem. B **121**, 3882 (2017).

[35] S. A. Grigoryev and L. B. Ioffe, FEBS Lett. **130**, 43 (1981).

[36] C. L. Woodcock, S. A. Grigoryev, R. A. Horowitz, and N. Whitaker, Proc. Natl. Acad. Sci. U.S.A. **90**, 9021 (1993).

[37] M. Wakamori, Y. Fujii, N. Suka, M. Shirouzu, K. Sakamoto, T. Umehara, and S. Yokoyama, Sci. Rep. **5**, 17204 (2015).

[38] P. J. Hagerman, Annu. Rev. Biophys. Biophys. Chem. **17**, 265 (1988).

[39] C. Bustamante, J. F. Marko, E. D. Siggia, and S. Smith, Science **265**, 1599 (1994).

[40] Z. Bryant, M. D. Stone, J. Gore, S. B. Smith, N. R. Cozzarelli, and C. Bustamante, Nature (London) **424**, 338 (2003).

[41] J. F. Marko and E. D. Siggia, Macromolecules **28**, 8759 (1995).

[42] A. J. Spakowitz, Europhys. Lett. **73**, 684 (2006).

[43] S. Mehraeen, B. Sudhanshu, E. F. Koslover, and A. J. Spakowitz, Phys. Rev. E **77**, 061803 (2008).

[44] Y. Zhou and G. S. Chirikjian, J. Chem. Phys. **119**, 4962 (2003).

[45] J. Yan and J. F. Marko, Phys. Rev. E **68**, 011905 (2003).

[46] See Supplemental Material at http://link.aps.org/supplemental/10.1103/PhysRevLett.123.208103 for detailed derivation of $B_{l_0 m_0 j_0}^{lmj}$, validation of numerical methods, examples of different unwrapping levels, and tables of effective Kuhn lengths.

[47] C. L. White, R. K. Suto, and K. Luger, EMBO J. **20**, 5207 (2001).

[48] T. J. Richmond and C. A. Davey, Nature (London) **423**, 145 (2003).

[49] J. Bednar *et al.*, Mol. Cell **66**, 384 (2017).

[50] S. Bilokapic, M. Strauss, and M. Halic, Sci. Rep. **8**, 7046 (2018).

[51] M. Eltsov, D. Grewe, N. Lemercier, A. Frangakis, F. Livolant, and A. Leforestier, Nucleic Acids Res. **46**, 9189 (2018).

[52] B.-R. Zhou, J. Jiang, H. Feng, R. Ghirlando, T. S. Xiao, and Y. Bai, Mol. Cell **59**, 628 (2015).

[53] P. Kilanowski, P. March, and M. Samara, arXiv:1711.04032.

[54] A. L. Sanborn, S. S. P. Rao, S.-C. Huang, N. C. Durand, M. H. Huntley, A. I. Jewett, I. D. Bochkov, D. Chinnappan, A. Cutkosky, J. Li, K. P. Geeting, A. Gnirke, A. Melnikov, D. McKenna, E. K. Stamenova, E. S. Lander, and E. L. Aiden, Proc. Natl. Acad. Sci. U.S.A. **112**, E6456 (2015).

[55] J. Shimada and H. Yamakawa, Macromolecules **17**, 689 (1984).

[56] Y. Liu, T. Pérez, W. Li, J. D. Gunton, and A. Green, J. Chem. Phys. **134**, 065107 (2011).

[57] P. A. Wiggins, R. Phillips, and P. C. Nelson, Phys. Rev. E: Stat. Nonlinear Soft Matter Phys. **71**, 021909 (2005).

[58] J. Langowski, Eur. Phys. J. E **19**, 241 (2006).

[59] F. Benedetti, D. Racko, J. Dorier, Y. Burnier, and A. Stasiak, Nucleic Acids Res. **45**, 9850 (2017).

[60] Q. MacPherson, B. Beltran, and A. J. Spakowitz, Proc. Natl. Acad. Sci. U.S.A. **115**, 12739 (2018).

[61] J. Nuebler, G. Fudenberg, M. Imakaev, N. Abdennur, and L. A. Mirny, Proc. Natl. Acad. Sci. U.S.A. **115**, E6697 (2018).

[62] S. K. Ghosh and D. Jost, PLoS Comput. Biol. **14**, e1006159 (2018).

[63] A. Rosa and R. Everaers, PLoS Comput. Biol. **4**, e1000153 (2008).

[64] C. A. Brackley, J. Johnson, D. Michieletto, A. N. Morozov, M. Nicodemi, P. R. Cook, and D. Marenduzzo, Phys. Rev. Lett. **119**, 138101 (2017).

[65] D. Michieletto, E. Orlandini, and D. Marenduzzo, Phys. Rev. X **6**, 041047 (2016).